Reaction Path Hamiltonian Analysis of Dynamical Solvent Effects for a Claisen Rearrangement and a Diels−Alder Reaction

Hong Hu, Mark N. Kobrak, Changsen Xu, and Sharon Hammes-Schiffer*

Department of Chemistry and Biochemistry, University of Notre Dame, Notre Dame, Indiana 46556

Received: February 3, 2000; In Final Form: May 18, 2000

The solvent effects for a Claisen rearrangement and a Diels−Alder reaction are investigated. Electronic structure methods are used to generate the frequencies, couplings, and curvatures along the minimum energy paths for these reactions in the gas phase and in the presence of two water molecules. The geometries and charge distributions along the minimum energy paths are analyzed to determine the structural and electrostatic roles of the water molecules. Reactive flux molecular dynamics methods based on a reaction path Hamiltonian are used to calculate the dynamical transmission coefficients, which account for recrossings of the transition state. The transmission coefficients for the Claisen rearrangement are nearly unity both in the gas phase and in the presence of two water molecules. The transmission coefficients for the Diels−Alder reaction are 0.95 and 0.89 in the gas phase and in the presence of two water molecules, respectively. These differences in the transmission coefficients are explained in terms of the locations and magnitudes of the curvature peaks along the reaction path, as well as the shape of the potential energy along the reaction coordinate near the transition state. Analysis of the dynamical trajectories provides insight into the dynamical role of the water molecules and elucidates possible reaction mechanisms.

I. Introduction

Solvent effects have been found to be significant for a number of fundamental organic reactions. For example, the reaction rates of both Claisen rearrangements and Diels−Alder reactions have been found to be accelerated in polar solvents. Experimental data suggest that the Claisen rearrangement of allyl vinyl ether is accelerated by as much as a factor of 1000 in water relative to the rate in the gas phase.[1−5] Moreover, experiments also indicate that the Diels−Alder reaction of cyclopentadiene with methyl vinyl ketone is accelerated by a factor of 730 in water relative to the rate in isooctane.[6,7]

Both the Claisen rearrangement of allyl vinyl ether and the Diels−Alder reaction of cyclopentadiene with methyl vinyl ketone have been studied with a wide range of computational methods. One approach has been to perform electronic structure calculations on the reacting system in the presence of a dielectric continuum solvent.[8−14] Typically these calculations are problematic because of the lack of consideration of explicit hydrogen bonding interactions. An alternative approach has been to perform Monte Carlo or molecular dynamics simulations for the reacting system in the presence of explicit solvent molecules. These calculations have been successful in reproducing experimentally measured free energies of solvation.

Jorgensen and co-workers performed pioneering simulations of these two reactions in the presence of explicit solvent molecules.[5,15−17] In these studies, electronic structure methods were used to generate the minimum energy path (MEP) in the gas phase. The geometries and partial charges along this MEP were incorporated into a molecular mechanical potential for the reacting system immersed in a periodic box of explicit solvent molecules. Monte Carlo simulations based on this potential energy surface were used to calculate free energies of solvation along the MEP. In related studies, Gao and co-workers used mixed quantum mechanical/molecular mechanical (QM/MM) methods to study both reactions.[18−20] These simulations differ from those of Jorgensen and co-workers in that solute electronic structure relaxation was allowed. Thus, the effect of solvent polarization on the reacting system was included explicitly. In both types of Monte Carlo simulations, however, the solute geometries were dictated by the gas phase MEP, and dynamical effects were neglected.

Pak and Voth have studied the dynamical effects of the Diels−Alder reaction of cyclopentadiene with methyl vinyl ketone.[21] In their studies, they developed an empirical potential energy surface allowing solute motion based on gas phase electronic structure calculations. They performed molecular dynamics simulations with this potential energy surface in the presence of explicit solvent molecules to calculate the activation free energy. In addition, they investigated dynamical effects using a reactive flux method.[22] Although this study represents an important achievement, this approach requires both the development of a multidimensional potential energy surface and significant computational resources.

The goal of this paper is to investigate the dynamical solvent effects for the Claisen rearrangement and the Diels−Alder reaction within the framework of the reaction path Hamiltonian (RPH) developed by Miller, Handy, and Adams.[23] This RPH characterizes the reaction in terms of motion along the MEP and vibrational motion orthogonal to this path, where the MEP is defined as the steepest-descent path in mass-weighted coordinates from the saddle point down toward reactants and toward products. The RPH depends on the potential energy, frequencies, and couplings along the MEP. As shown previously,[24−26] electronic structure methods can be used to generate these quantities along the MEPs for chemical reactions. In this paper, we generate these quantities for the reactions in the gas phase and in the presence of a small number of explicit water molecules. Moreover, the geometries and partial charges along the MEP are analyzed to elucidate the structural and electrostatic roles of the water molecules.

10.1021/jp000449e CCC: $19.00
Published on Web 08/03/2000

In addition to these electronic structure calculations, we also use reactive flux molecular dynamics methods based on the RPH to calculate the dynamical transmission coefficients, which account for recrossings of the transition state. In these reactive flux calculations, a flux-weighted canonical distribution of classical molecular dynamics trajectories is started at the transition state and propagated backward and forward in time. The recrossings of the transition state are monitored to determine the transmission coefficient using the prescription of Keck.[27−29] The transmission coefficient provides an indication of deviations from transition state theory due to dynamical recrossings of the transition state. Moreover, analysis of the dynamical trajectories provides insight into the dynamical role of the water molecules and elucidates possible reaction mechanisms. The advantage of this approach is that useful information about dynamical solvent effects is obtained in a computationally tractable way.

The organization of this paper is as follows. In section II, we discuss the electronic structure methods, the reaction path Hamiltonian, and the reactive flux molecular dynamics method used in our calculations. In section III, we present the results and analyses for both the Claisen rearrangement and the Diels−Alder reaction. Concluding remarks are presented in section IV.

II. Methods

The electronic structure calculations were carried out with the Gaussian 98 program[30] using the restricted Hartree−Fock (RHF) method, second-order Moller−Plesset perturbation theory (MP2), and density functional theory (DFT). The basis set used in all of these calculations is the standard 6-31G** basis set.[31−33] The functional used in all DFT calculations is the hybrid functional B3LYP.[34−37] At all three levels of theory, the reactant, transition state, and product structures were determined for the reaction in the gas phase and in the presence of two water molecules. At the RHF/6-31G** and DFT/B3LYP/6-31G** levels, the minimum energy paths (MEPs) to the associated reactant and product were generated using the method of Schlegel and co-workers.[38,39] The transition state searches were carried out with the "OPT = VeryTight" option, and the MEPs were constructed with the "IRC = VeryTight" option and a step size of 0.05 amu$^{1/2}$ bohr. The partial charges were calculated for the reactant, transition state, and product structures using the CHELPG method.[40] The entropy and zero point energy contributions to the energy barriers were calculated using the frequencies of the reactant and transition state structures with the standard approximations implemented in Gaussian 98.[30]

The MEPs were analyzed within the framework of the RPH developed by Miller, Handy, and Adams.[23] This RPH is expressed in terms of the reaction coordinate s and its conjugate momentum p_s, as well as the coordinates and momenta $\{Q_k, P_k\}$ ($k = 1, ..., F - 1$) of the orthogonal vibrational modes. Here, $F = 3N - 6$ is the number of vibrational degrees of freedom of a nonrotating N-atom system, and the Fth degree of freedom is defined to be the reaction coordinate s. For zero total angular momentum, the RPH is

$$H(p_s, s, \{P_k, Q_k\}) = \frac{1}{2}\frac{\left[p_s - \sum_{k,l=1}^{F-1} Q_k P_l B_{k,l}(s)\right]^2}{\left[1 + \sum_{k=1}^{F-1} Q_k B_{k,F}(s)\right]^2} + \sum_{k=1}^{F-1}\left[\frac{1}{2}P_k^2 + \frac{1}{2}\omega_k(s)^2 Q_k^2\right] + V_o(s) \qquad (1)$$

Here, $\omega_k(s)$ is the frequency of mode k, and $B_{k,l}$ is the coupling, defined as

$$B_{k,l}(s) = \frac{d\mathbf{L}_k(s)}{ds}\cdot\mathbf{L}_l(s) \qquad (2)$$

where $\mathbf{L}_k(s)$ ($k = 1, ..., F - 1$) and $\mathbf{L}_F(s)$ denote the kth normal mode vector and the normalized gradient vector, respectively, at s. The squared frequencies $\omega_k(s)^2$ and the normal mode vectors $\mathbf{L}_k(s)$ ($k = 1, ..., F - 1$) are the eigenvalues and eigenvectors, respectively, of the Hessian matrix at s from which infinitesimal translations and rotations and the gradient vector $\mathbf{L}_F(s)$ have been projected. Note that $B_{k,l}(s)$ ($k,l = 1, ..., F - 1$) are the coupling elements between normal modes Q_k and Q_l, and $B_{k,F}(s)$ ($k = 1, ..., F - 1$) are the coupling elements between the normal mode Q_k and the reaction coordinate s. As described in ref 23, the coupling elements in the denominator of the first term of eq 1 describe the effects of reaction path curvature, where the curvature is defined as $[\sum_{k=1}^{F-1} B_{k,F}(s)^2]^{1/2}$. We obtained the frequencies $\omega_k(s)$ and the eigenvectors $\mathbf{L}_k(s)$ along the MEPs using the "Freq = (Projected, HPmodes)" option in Gaussian 98.[30] Subsequently, we calculated the couplings $B_{k,l}(s)$ and the curvature with our own program.

To simplify our molecular dynamics calculations based on the RPH, we analyzed the orthogonal vibrational modes and included only those modes strongly coupled to the reaction coordinate. The frequencies and eigenvectors of the orthogonal vibrational modes obtained from Gaussian 98 are labeled from low to high frequency. Note that this labeling scheme does not correspond to the physical identity of the modes (i.e., the frequencies of the physically meaningful modes may cross). We determined the physically meaningful modes by calculating the dot products between the normal mode vectors at various points along the MEP and used a spline interpolation scheme[41] to smoothly follow the pathways that maximize the dot products. In this way, we generated a set of physically meaningful orthogonal vibrational modes and calculated the coupling of these modes to the reaction coordinate. In our dynamical calculations we included only the physically meaningful orthogonal vibrational modes that exhibited coupling to the reaction coordinate larger than 0.1 amu$^{-1/2}$ bohr^{-1}. For simplicity, we neglected the coupling between these orthogonal modes. Analytical forms for the energy $V_o(s)$ along the reaction path and for the frequencies $\omega_k(s)$ and couplings $B_{k,F}(s)$ of the included modes were obtained by fitting to linear combinations of Gaussian functions.

The transmission coefficient κ for each system was calculated using Keck's method.[27−29] In this approach, κ is calculated as the flux-weighted average of ξ for an ensemble of classical molecular dynamics trajectories started at the dividing surface and integrated backward and forward in time. The factor ξ corrects for multiple crossings of the dividing surface (i.e., so that all trajectories that originate as reactants and end as products are counted only once, no matter how many times they cross the dividing surface, and all trajectories that go from reactants to reactants, products to products, or products to reactants are not counted at all). In particular, $\xi = 1/\alpha$ for trajectories that have α forward crossings and $\alpha - 1$ backward crossings of the dividing surface, and ξ is zero otherwise.

In our calculations of the transmission coefficient, we propagated an ensemble of 10 000 trajectories started at the dividing surface (defined as $s = 0$) for each system studied. The initial conditions for the velocities and the orthogonal mode coordinates of each trajectory were generated assuming a

TABLE 1: Energy Barriers for the Claisen Rearrangement

method	ΔE (kcal/mol)
B3LYP/6-311+G** [a]	26.1
MP2/6-31G* [b]	26.2
RHF/6-31G** [c]	47.6
DFT/B3LYP/6-31G** [c]	27.4

[a] Reference 48. [b] Reference 13. [c] This paper.

Boltzmann distribution in both kinetic and potential energy. The temperature for all simulations was 298 K. Couplings between the reaction coordinate and the orthogonal modes were assumed to be zero for this assignment (i.e., each orthogonal mode was treated as an uncoupled harmonic oscillator). The classical equations of motion were derived from the RPH given in eq 1 using the usual relations[42] and were numerically integrated using a fourth-order Runge−Kutta scheme.[41] We used an integration time step of $\delta t = 0.012$ fs. We confirmed the convergence of our results with respect to time step and number of trajectories.

As discussed previously,[24,43,44] the RPH in eq 1 is singular when $\sum_{k=1}^{F-1} Q_k B_{k,F}(s) = -1$. This singularity can be eliminated by approximating the term $1/[1 + \sum_{k=1}^{F-1} Q_k B_{k,F}(s)]$ as a power series around $\sum_{k=1}^{F-1} Q_k B_{k,F}(s) = 0$ and retaining only the terms linear in the coupling $B_{k,F}(s)$.[43,44] If a classical trajectory approaches the singularity, however, the trajectory is outside the region in which the series expansion is valid so the result is meaningless even if not numerically singular. In other words, the RPH approach breaks down at the singularity. Therefore, rather than attempting to approximate the Hamiltonian and remove the singularity, we chose instead to integrate the full equations of motion and discard all trajectories that encounter numerical difficulties. Thus, any trajectory in which energy is not conserved to one part in 10^5 was discarded. As will be shown below, for the systems studied in this paper very few trajectories approached singular configurations.

III. Results

A. Claisen Rearrangement. The first reaction studied was the Claisen rearrangement of allyl vinyl ether.

We optimized the reactant, transition state, and product structures at the RHF/6-31G** and DFT/B3LYP/6-31G** levels. Since the chair transition state has been found to be significantly lower in energy than the boat transition state[45] and has been used for previous solvation studies,[5,14,18] we focused on only the chair transition state. As shown in Table 1, the DFT/B3LYP/6-31G** barrier height agrees well with previous DFT/B3LYP calculations and MP2 calculations. In contrast, the RHF/6-31G** method significantly overestimates the barrier height. Thus, the remaining calculations discussed in this section utilize the DFT/B3LYP/6-31G** method.

We calculated the MEPs for the reaction in the gas phase and for the reaction in the presence of two water molecules. We found several transition states in the presence of two water molecules. We chose to use the transition state in which both water molecules are hydrogen-bonded to the oxygen atom of the solute but are not hydrogen-bonded to each other. Although there may be lower energy structures in which the two water molecules are hydrogen-bonded to each other, simulation studies suggest that our chosen transition state is most relevant to the situation in bulk solvent.[5,14] Figure 1 depicts the reactant, transition state, and product structures in the presence of the two water molecules. As indicated by previous calculations,[5,18] the transition state is stabilized by enhanced hydrogen bonding of the water molecules to the solute oxygen.

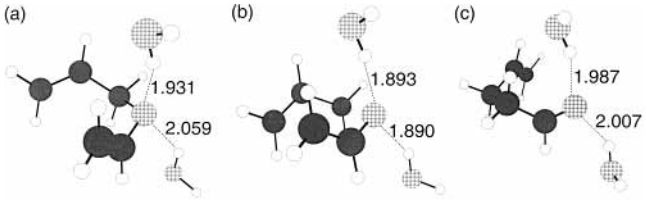

Figure 1. Optimized structures of the (a) reactant, (b) transition state, and (c) product for the Claisen rearrangement in the presence of two water molecules. The carbon atoms are solid gray, the hydrogen atoms are solid white, and the oxygen atoms are checkered. Hydrogen bonding distances between the water molecules and the solute oxygen atom are indicated.

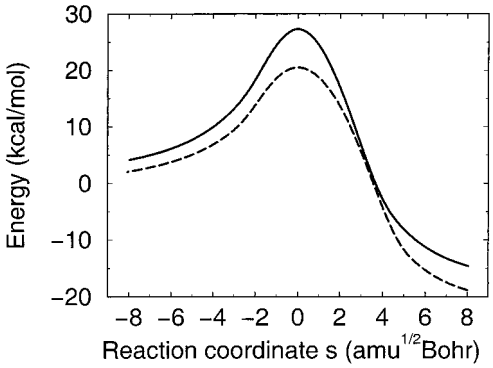

Figure 2. Minimum energy paths for the Claisen rearrangement in the gas phase (solid) and in the presence of two water molecules (dashed). For both curves, the energies are measured relative to the optimized reactant.

Figure 2 depicts the energies along the MEPs in the gas phase and in the presence of two water molecules. The energy barrier (i.e., the difference in energy between the transition state and the reactant) is lowered by 6.8 kcal/mol by the presence of the two water molecules. Accounting for entropy and zero point energy effects, the free energy of solvation due to the two water molecules is −6.0 kcal/mol. The inclusion of only two water molecules does not account for collective solvent effects, such as disrupting the hydrogen-bonding network of water in creating a cavity. Nevertheless, the degree of solvation is qualitatively similar to values for the free energies of solvation obtained experimentally[3−5,14] and with a variety of other theoretical methods.[5,8,14,18]

We also studied the geometries and partial charges along the MEPs. The results for the reactant and transition state structures are presented in Tables 2 and 3. Table 2 indicates that, for both the reactant and the transition state, the C_2-O and C_4-O bonds are slightly longer in the presence of the two water molecules. This lengthening is expected because of the hydrogen bonding of the solute oxygen to the water molecules. We observed that the lengthening of the C_4-O bond is more pronounced for the transition state structure. Moreover, the C_6-C_1 bond increases for the transition state but decreases for the reactant in the presence of the two water molecules. (Note that the C_4-O and C_6-C_1 bonds are formed and broken during the Claisen rearrangement.) Thus, solvation causes the transition state to be looser and more dissociative.[14] The partial charges indicate that, for both the reactant and transition state, approximately −0.15 of an electron charge is transferred to the two water

TABLE 2: Bond Lengths[a] for the Claisen Rearrangement Reactant and Transition State at the DFT/B3LYP/6-31G Level in the Gas Phase and in the Presence of Two Water Molecules**

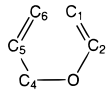

	reactant (gas phase)	reactant (with 2 waters)	transition state (gas phase)	transition state (with 2 waters)
C_1-C_2	1.332	1.328	1.383	1.371
C_2-O	1.366	1.385	1.287	1.308
$O-C_4$	1.433	1.454	1.914	1.979
C_4-C_5	1.503	1.499	1.401	1.402
C_5-C_6	1.332	1.332	1.382	1.375
C_6-C_1	5.074	4.713	2.322	2.463

[a] Bond lengths are in angstroms.

TABLE 3: Partial Charges[a] for the Claisen Rearrangement Reactant and Transition State at the DFT/B3LYP/6-31G Level in the Gas Phase and in the Presence of Two Water Molecules**

	reactant (gas phase)	reactant (with 2 waters)	transition state (gas phase)	transition state (with 2 waters)
C_1	−0.16	−0.08	−0.06	−0.05
C_2	+0.25	+0.16	+0.26	+0.22
O	−0.31	−0.18	−0.39	−0.32
C_4	+0.27	+0.34	+0.21	+0.22
C_5	+0.02	−0.02	−0.13	−0.03
C_6	−0.06	−0.05	+0.11	+0.10

[a] Partial charges include attached hydrogens.

molecules. The magnitude of the charge on the solute oxygen decreases in the presence of the water molecules because of this transfer of negative charge to the water molecules. The calculated charges on the oxygen atoms indicate, however, that the presence of the water molecules increases the polarity of the transition state more than that of the reactant. (The presence of the water molecules changes the charge on the oxygen from −0.39 to −0.32 for the transition state and from −0.31 to −0.18 for the reactant, indicating greater polarity of the transition state.)

We have analyzed the MEPs within the framework of the RPH. Panels a and b of Figure 3 depict the frequencies of the orthogonal vibrational modes along the MEP for the reaction in the gas phase and in the presence of two water molecules, respectively. Figure 4a depicts the curvature along the MEP for the reaction in the gas phase (solid) and in the presence of two water molecules (dashed). The sharp peak in the curvature at $s = 0$ is assumed to be a numerical artifact. This sharp peak arises from the sum of the small peaks at $s = 0$ for all vibrational modes caused by numerical errors at the transition state. Thus, the meaningful curvature consists of the two peaks on the reactant and product sides depicted in Figure 4a.

The presence of the two water molecules increases the overall curvature by ∼10% and shifts the peaks slightly away from $s = 0$. The increase in curvature is due to the coupling of the water molecules to the reaction coordinate. In the gas phase, the strongly coupled modes contain contributions from the stretching motion of the C_4-O and C_1-C_6 bonds, which are broken and formed during the reaction. In the presence of the two water molecules, the strongly coupled modes still contain these contributions but also contain contributions from the stretching motion of the hydrogen bonds between the water molecules and the solute oxygen.

We have calculated the dynamical transmission coefficient κ using the methodology described in section II. The solid lines in Figure 3 indicate the orthogonal vibrational modes used in our calculations. Two orthogonal modes were included in the gas phase calculations, and three orthogonal modes were included in the calculations with two explicit water molecules.

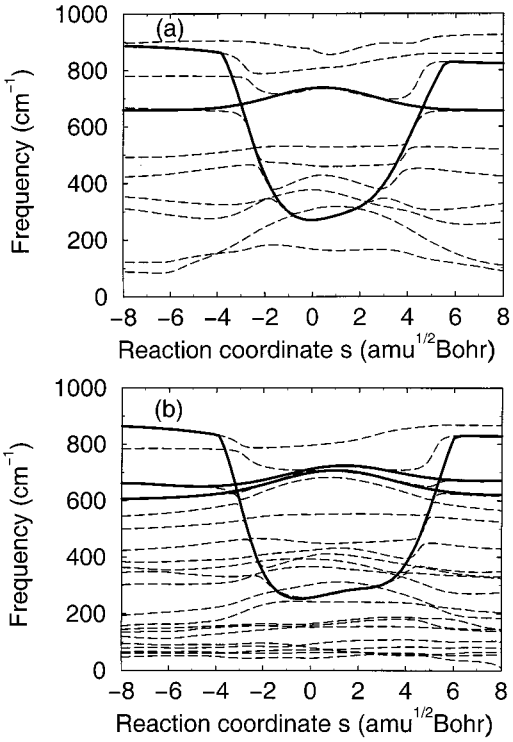

Figure 3. Frequencies of the orthogonal vibrational modes along the MEP for the Claisen rearrangement (a) in the gas phase and (b) in the presence of two water molecules. The frequencies labeled from low to high (up to 1000 cm^{-1}) are shown by dashed lines. The orthogonal vibrational modes included in the dynamical calculations are indicated by solid lines.

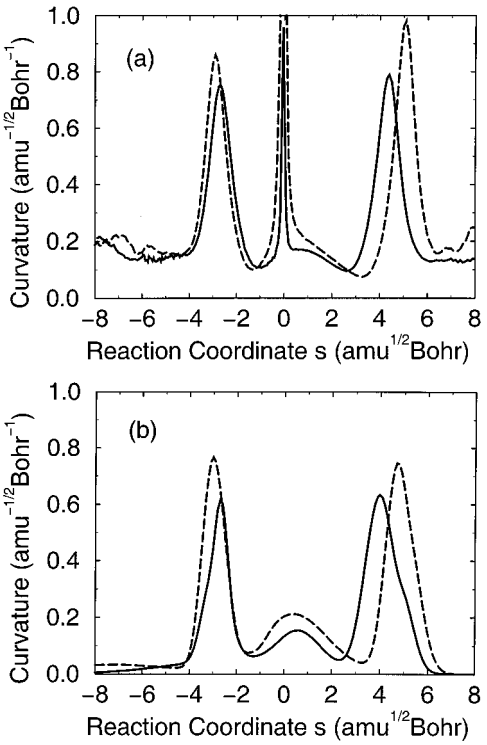

Figure 4. (a) Curvature along the MEP for the Claisen rearrangement in the gas phase (solid) and in the presence of two water molecules (dashed); (b) Same as panel a but including only the dominant orthogonal modes indicated in Figure 3.

TABLE 4: Results of Dynamical Simulations for the Claisen Rearrangement and the Diels−Alder Reaction

	$\Delta G^{\ddagger}$ [a]	κ [b]	κ_-/κ_+ [c]	θ_{ref} [d]	θ_{rec} [e]	θ_{sing} [f]
Claisen	28.3	0.995	0.992/0.995	0.081	0.000	0.003
Claisen/2H_2O	22.3	0.991	0.927/0.992	0.093	0.000	0.056
Diels−Alder	22.9	0.950	n/a	0.088	0.051	0.000
Diels−Alder/2H_2O	17.7	0.892	0.881/0.894	0.133	0.038	0.009

[a] $\Delta G^{\ddagger}$ is the free energy barrier in kilocalories per mole calculated with the inclusion of zero point energy and entropy effects. [b] κ denotes the transmission coefficient derived when all singular trajectories were ignored. [c] κ_+ denotes an upper limit on the value of κ in which all singular trajectories were assumed to move directly from reactant to product, and κ_- is a lower limit based on the assumption that none of the discarded trajectories contributed to the reactive flux. [d] θ_{ref} is the fraction of numerically stable trajectories that were unsuccessful due to reflections. [e] θ_{rec} is the fraction of numerically stable trajectories that crossed the dividing surface in the forward direction more than once. [f] θ_{sing} is the fraction of numerically unstable trajectories.

The curvatures obtained from including only these modes are shown in Figure 4b. Note that the magnitudes of the peaks in Figure 4b are somewhat lower than the magnitudes of the full curvature peaks shown in Figure 4a. Although we included all orthogonal modes with couplings to the reaction coordinate larger than 0.1 amu$^{-1/2}$ bohr^{-1}, the sum of many small couplings accounts for the difference between Figure 4a and b. By varying the parameters in our functional representation of the couplings, we found that the transmission coefficient is insensitive to these differences in curvature (although the number of discarded trajectories due to the singularity in the RPH increases as the curvature increases).

As shown in Table 4, the transmission coefficient is very close to unity for the Claisen rearrangement in the gas phase and in the presence of two water molecules. The deviations of the transmission coefficient from unity are due solely to unsuccessful trajectories (i.e., trajectories that started and ended in reactants, started and ended in products, or started in products and ended in reactants) resulting from reflections. In this paper, reflections are defined to be changes in the sign of the momentum along the reaction coordinate caused by interactions between the reaction coordinate and an orthogonal vibrational mode. Repeated reflections could lead to successful trajectories that exhibit recrossings of the dividing surface in the forward direction. For the Claisen reactions, however, no such forward recrossings occurred, despite the presence of a curvature peak on both the reactant and the product side. The lack of forward recrossings and the small number of reflections are due to a combination of the steep slope of the potential energy along the reaction coordinate and the relatively large distance of the curvature peaks from the transition state. When the trajectories move from the transition state to these curvature peaks, they acquire a large amount of momentum along the reaction coordinate, so reflections are unlikely. Note that very few trajectories were eliminated due to the singularity.

Although the transmission coefficient is nearly unity, we analyzed the dynamical behavior of individual trajectories to gain insight into possible dynamical mechanisms. Typically only trajectories with very low initial velocities along the reaction coordinate exhibited reflections. In some cases, the coupling peaks on the reactant or product side impacted the dynamical trajectories, as shown in the sample trajectory in Figure 5a. This trajectory leaves the reactant region with insufficient momentum along the reaction coordinate to reach the transition state. During its return to the reactant region, however, the trajectory is reflected because of coupling between the reaction coordinate and an orthogonal vibrational mode. The trajectory obtains

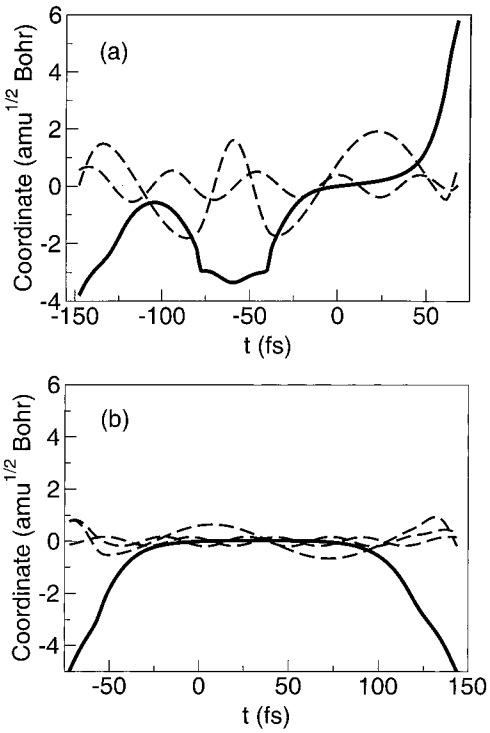

Figure 5. Sample trajectories from the dynamical calculations for the Claisen rearrangement (a) in the gas phase and (b) in the presence of two water molecules. The reaction coordinate s (solid) and the orthogonal modes Q_k (dashed) are shown as functions of time.

enough momentum from this coupling interaction to pass successfully through the transition state to the product side. In other cases, the trajectories are reflected because of coupling near the transition state, as shown in Figure 5b. This trajectory spends a significant amount of time at the transition state and is eventually reflected back to the reactant side, leading to an unsuccessful trajectory. Despite the relatively low curvature at the transition state, the low frequency of the orthogonal mode allows for a large displacement of this orthogonal coordinate. Since the RPH includes the product $B_{k,F}(s)Q_k$, a large displacement can lead to significant effective coupling near the transition state.

B. Diels−Alder Reaction. The second reaction studied was the Diels−Alder reaction of cyclopentadiene with methyl vinyl ketone.

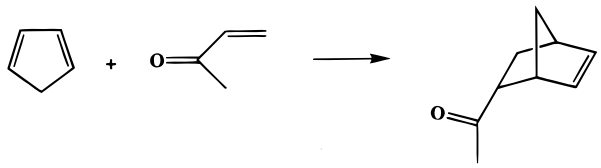

We optimized the reactant, transition state, and product structures at the RHF/6-31G**, MP2/6-31G**, and DFT/B3LYP/6-31G** levels. The endo-cis transition state structure was selected for our studies because this structure was previously found to be lowest in energy for gas phase Diels−Alder reactions[15,46,47] and was used in previous solvation studies.[15,16,20] As shown in Table 5, the DFT/B3LYP/6-31G** energy barrier agrees well with the results of higher-level calculations reported in ref 21. In contrast, the RHF/6-31G** method overestimates the barrier height, and the MP2/6-31G** method underestimates it. Thus, the remaining calculations discussed in this section utilize the DFT/B3LYP/6-31G** method.

TABLE 5: Energy Barriers for the Diels−Alder Reaction

method	ΔE (kcal/mol)
B3LYP/6-31+G*[a]	16.3
MP4SDQ[a]	17.7
CCSD[a]	18.0
RHF/6-31G**[b]	36.1
MP2/6-31G**[b]	7.21
DFT/B3LYP/6-31G**[b]	17.0

[a] Reference 21, where the MP4SDQ and CCSD values were calculated for the B3LYP/6-31+G* optimized geometries. [b] This paper.

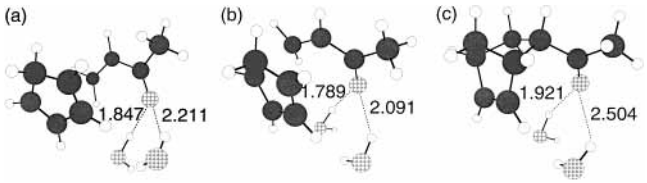

Figure 6. Optimized structures of the (a) reactant, (b) transition state, and (c) product for the Diels−Alder reaction in the presence of two water molecules. The carbon atoms are solid gray, the hydrogen atoms are solid white, and the oxygen atoms are checkered. Hydrogen bonding distances between the water molecules and the solute oxygen atom are indicated.

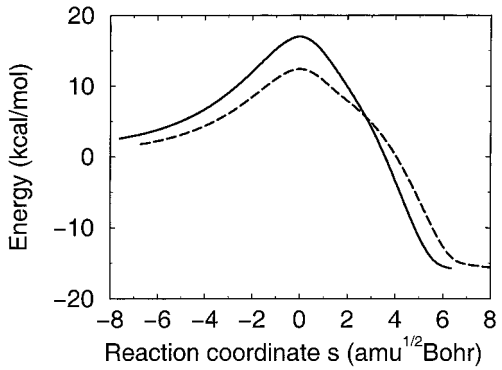

Figure 7. Minimum energy paths for the Diels−Alder reaction in the gas phase (solid) and in the presence of two water molecules (dashed). For both curves, the energy is measured relative to the optimized reactant.

We calculated the MEPs for the reaction in the gas phase and for the reaction in the presence of two water molecules. We chose the lowest-energy endo-cis transition state found in the presence of two water molecules, which coresponds to the water molecules hydrogen-bonded to the solute oxygen and hydrogen-bonded to each other. Note that the alternative transition state without hydrogen bonding between the two water molecules may be more representative of the situation in bulk solvent. (Simulations suggest that this is the case for the Claisen rearrangement described above.) In the absence of evidence that this is the case for the Diels−Alder reaction, however, we chose the lowest energy transition state. Figure 6 depicts the reactant, transition state, and product structures in the presence of the two water molecules. As indicated by previous calculations,[15,16,20] the transition state is stabilized by enhanced hydrogen bonding of the water molecules to the solute oxygen.

The energies along the MEPs in the gas phase and in the presence of two water molecules are depicted in Figure 7. The energy barrier is lowered by 4.6 kcal/mol due to the presence of the two water molecules. Accounting for entropy and zero point energy effects, the free energy of solvation due to the two water molecules is −5.2 kcal/mol. Despite the neglect of collective solvent effects, this result agrees qualitatively with solvation energies obtained experimentally[6,7] and from previous calculations.[15,16,20,21]

TABLE 6: Bond Lengths[a] for the Diels−Alder Reactant and Transition State at the DFT/B3LYP/6-31G Level in the Gas Phase and in the Presence of Two Water Molecules**

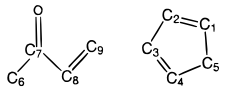

	reactant (gas phase)	reactant (with 2 waters)	transition state (gas phase)	transition state (with 2 waters)
C_1-C_2	1.350	1.351	1.409	1.408
C_2-C_3	1.470	1.470	1.407	1.413
C_3-C_4	1.349	1.350	1.383	1.379
C_4-C_5	1.506	1.507	1.502	1.501
C_5-C_1	1.506	1.506	1.520	1.520
C_6-C_7	1.515	1.510	1.523	1.519
C_7-C_8	1.496	1.483	1.460	1.437
C_8-C_9	1.336	1.339	1.399	1.403
C_7-O	1.222	1.232	1.233	1.251
C_1-C_9	4.356	6.278	2.020	2.013
C_4-C_8	4.191	4.665	2.608	2.744

[a] Bond lengths are in angstroms.

TABLE 7: Partial Charges[a] for the Diels−Alder Reactant and Transition State at the DFT/B3LYP/6-31G Level in the Gas Phase and in the Presence of Two Water Molecules**

	reactant (gas phase)	reactant (with 2 waters)	transition state (gas phase)	transition state (with 2 waters)
C_1	−0.19	−0.21	+0.08	+0.04
C_2	+0.07	+0.07	−0.01	+0.06
C_3	−0.01	+0.06	+0.02	+0.02
C_4	−0.17	−0.22	+0.00	+0.01
C_5	+0.29	+0.29	+0.06	+0.08
C_6	−0.05	−0.05	−0.09	−0.11
C_7	+0.58	+0.68	+0.61	+0.74
C_8	−0.16	−0.19	−0.27	−0.39
C_9	+0.09	+0.12	+0.11	+0.19
O	−0.46	−0.54	−0.51	−0.62

[a] Partial charges include attached hydrogens.

We also studied the geometries and partial charges along the MEPs in the gas phase and in the presence of the two water molecules. The values obtained for the reactant and transition state structures are given in Tables 6 and 7. Table 6 indicates that the C_7-O bond is slightly longer in the presence of the two water molecules than in the gas phase for both the reactant and transition state and is slightly larger in the transition state than in the reactant. Moreover, as expected, the C_1-C_9 and C_4-C_8 bonds, which are formed during the reaction, are much longer in the reactant than in the transition state. In the transition state, the C_1-C_9 bond is not significantly affected by the two water molecules, but the C_4-C_8 bond is 0.14 Å longer in the presence of the two water molecules than in the gas phase. Thus, as for the Claisen rearrangement, the two water molecules lead to a looser, more dissociative transition state. Table 7 indicates that, in contrast to the Claisen rearrangement, only −0.01 of an electron charge is transferred to the two water molecules for the reactant and transition state. The smaller amount of charge transferred for the Diels−Alder reaction than for the Claisen rearrangement could be due to the hydrogen bonding between the two water molecules that is present for the Diels−Alder but not for the Claisen transition state. This hydrogen bonding between the two water molecules decreases the strength of the hydrogen bonding to the solute and thus could decrease the amount of charge transferred between the solute and the two water molecules. As a result of the small amount of negative charge transferred to the two water molecules, Table 7 indicates

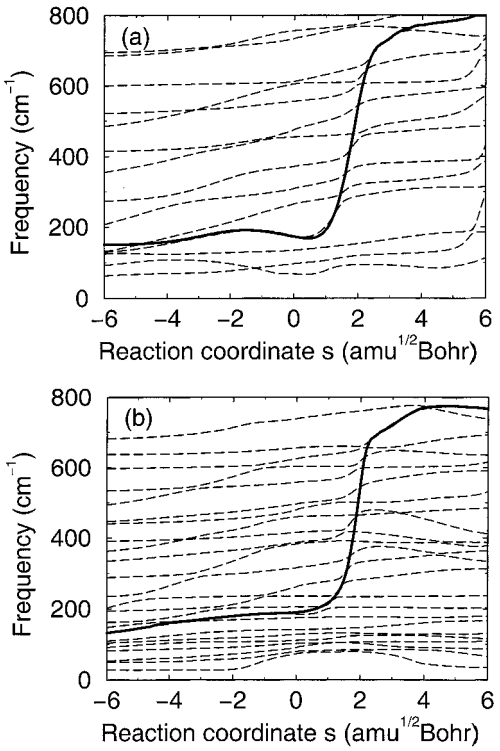

Figure 8. Frequencies of the orthogonal vibrational modes along the MEP for the Diels−Alder reaction (a) in the gas phase and (b) in the presence of two water molecules. The frequencies labeled from low to high (up to 1000 cm^{-1}) are shown by dashed lines. The orthogonal vibrational modes included in the dynamical calculations are indicated by solid lines.

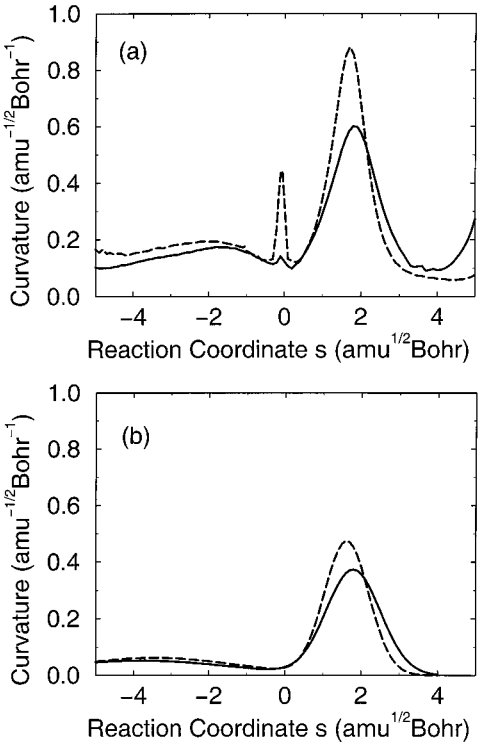

Figure 9. (a) Curvature along the MEP for the Diels−Alder reaction in the gas phase (solid) and in the presence of two water molecules (dashed). (b) Same as panel a but including only the dominant orthogonal modes indicated in Figure 8.

that the charge on the oxygen atom becomes more negative in the presence of the two water molecules for both the reactant and the transition state. The presence of the two water molecules changes the charge on the oxygen from −0.46 to −0.54 for the reactant and from −0.51 to −0.62 for the transition state. These charges show that the transition state is more polar than the reactant and that the two water molecules increase the polarity of the solute.

We have analyzed the MEPs within the framework of the RPH. Panels a and b of Figure 8 depict the frequencies of the orthogonal vibrational modes along the MEP for the reaction in the gas phase and in the presence of two water molecules, respectively. Figure 9a depicts the curvature along the MEP for the reaction in the gas phase (solid) and in the presence of two water molecules (dashed). As discussed above for the Claisen rearrangement, the peak at $s = 0$ is assumed to be a numerical artifact. Recall that, for the Claisen rearrangement, curvature peaks were observed on both the reactant and the product sides. For the Diels−Alder reaction, the meaningful curvature is found on the product side at $s \approx 1.9$ amu$^{1/2}$ bohr. The presence of the two water molecules shifts the curvature slightly toward $s = 0$ and increases the magnitude by ∼19% (due to the coupling of the water molecules to the reaction coordinate). In the gas phase, the strongly coupled modes contain contributions from the stretching of the bonds that are broken and formed during the reaction. In the presence of the two water molecules, the strongly coupled modes still contain these contributions but also contain contributions from the stretching motion of the hydrogen bonds between the water molecules and the solute oxygen. Note that the solvation increases the curvature more for the Diels−Alder reaction than for the Claisen rearrangement, indicating that the water molecules are more strongly coupled to the reaction coordinate for the Diels−Alder reaction.

We have calculated the dynamical transmission coefficient κ using the methodology described in section II. The solid lines in Figure 8 indicate the orthogonal vibrational modes used in our calculations. Only one orthogonal mode was included for the reactions in the gas phase and in the presence of two water molecules. The curvatures obtained from including only this single mode are shown in Figure 9b. As for the Claisen rearrangement, the magnitudes of the peaks in Figure 9b are somewhat lower than the magnitudes of the full curvature peaks shown in Figure 9a. Again, we found that the transmission coefficients are insensitive (to within ∼2%) to these differences in curvature.

Table 4 shows that the transmission coefficients for the Diels−Alder reactions are smaller than those for the Claisen rearrangement. Moreover, in contrast to the Claisen rearrangement, the Diels−Alder reaction exhibited forward recrossings of the transition state. These differences are caused by three factors. First, the potential energy surface along the reaction coordinate is flatter for the Diels−Alder reaction (especially in the presence of two water molecules), so the system does not acquire as much kinetic energy as it leaves the transition state. Second, the curvature peak is closer to the transition state for the Diels−Alder reaction, further reducing the kinetic energy in the reaction coordinate when the trajectory passes through the region of strong coupling. Third, the frequency of the orthogonal mode at the transition state is slightly smaller for the Diels−Alder reaction, allowing for larger displacements and thus larger values of the product $B_{k,F}(s)Q_k$. Table 4 also indicates that the transmission coefficient for the Diels−Alder reaction in the presence of two water molecules ($\kappa = 0.89$) is significantly smaller than that in the gas phase ($\kappa = 0.95$). The lower transmission coefficient in the presence of the water molecules is due to the flatter potential energy surface along the reaction coordinate near the transition state (as shown in Figure 7) and to the larger curvature peak on the product side (as shown in

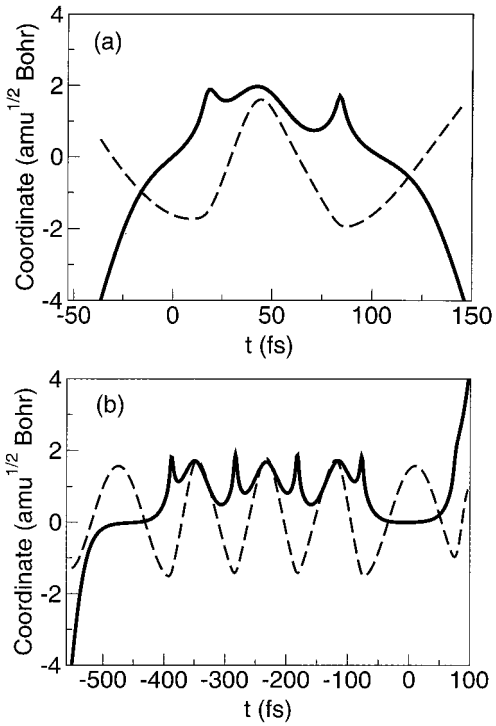

Figure 10. Sample trajectories from the dynamical calculations for the Diels−Alder reaction (a) in the gas phase and (b) in the presence of two water molecules. The reaction coordinate s (solid) and the orthogonal mode Q_k (dashed) are shown as functions of time.

Figure 9) in the presence of two water molecules. Note that the transmission coefficient of 0.89 reported in this paper is larger than the value of 0.67 calculated by Voth and co-workers for the same Diels−Alder reaction in aqueous solution. This discrepancy is due to the inclusion of only two water molecules in our calculations. Future work will be directed at including more solvent molecules by immersing the solute in a periodic box of hundreds of explicit solvent molecules. In this case, the transmission coefficient will be calculated by combining the RPH approach with a molecular mechanical description of the solvent molecules.

To gain insight into the possible dynamical mechanisms for the Diels−Alder reaction, we analyzed the dynamical behavior of individual trajectories. As for the Claisen rearrangement, typically reflections (and forward recrossings in this case) were observed only for trajectories with low initial velocities along the reaction coordinate. For the Diels−Alder reaction, the absence of a coupling peak on the reactant side prevented interactions in the reactant region. On the other hand, the close proximity of the existing coupling peak to the transition state, together with the flatter potential energy along the reaction coordinate near the transition state, resulted in stronger coupling and a higher probability of forward recrossings or reflections. Figure 10a depicts a trajectory that is unsuccessful because of reflection by the coupling peak on the product side. Figure 10b depicts a trajectory that is successful despite repeated reflections by the coupling peak on the product side. This trajectory crosses the dividing surface in the forward direction two times (at $t = -436$ fs and at $t = 0$ fs). This forward recrossing is due to the significant effective coupling $B_{k,F}Q_k$ at the transition state resulting from the large displacement of the orthogonal coordinate Q_k at the transition state. Thus, this trajectory illustrates that recrossings of the dividing surface can occur even in the absence of a coupling peak on the reactant side.

IV. Summary and Conclusions

This paper presents calculations aimed at elucidating the dynamical solvent effects for a Claisen rearrangement and a Diels−Alder reaction. Electronic structure methods were used to generate the minimum energy paths for the reactions in the gas phase and in the presence of two water molecules. The structures and charge distributions along these minimum energy paths were analyzed. The hydrogen bonding of the two water molecules to the solute oxygen atom was found to be stronger in the transition states than in the reactants. This enhanced hydrogen bonding accounts for the majority of the free energy of solvation. In addition, the presence of the two water molecules resulted in looser, more dissociative and more polarized transition states.

These minimum energy paths were also analyzed within the framework of the reaction path Hamiltonian. The curvatures, frequencies, and couplings along the minimum energy paths were calculated for the reactions in the gas phase and in the presence of two water molecules. The Claisen rearrangement exhibits curvature peaks on both the reactant and the product sides. In contrast, the Diels−Alder reaction exhibits only a peak on the product side. For both reactions, the presence of the two water molecules increases the overall curvature due to the coupling of the solvent motion to the reaction coordinate. Moreover, for both reactions, the strongly coupled modes in the gas phase were found to contain contributions from the stretching motion of bonds that are broken and formed during the reaction. In the presence of two water molecules, the strongly coupled modes were found to contain additional contributions from the stretching motion of the hydrogen bonds between the water molecules and the solute oxygen.

Reactive flux calculations based on the RPH were used to calculate the transmission coefficients, which account for recrossings of the transition state. Due to the locations of the coupling peaks, reflections occur in both the reactant and the product regions for the Claisen rearrangement but only in the product region for the Diels−Alder reaction. (For both reactions, reflections may also occur in the transition state region.) Recrossings of the transition state in the forward direction were observed for the Diels−Alder reaction but not for the Claisen rearrangement. The transmission coefficients were nearly unity for the Claisen rearrangement both in the gas phase and in the presence of two water molecules. In contrast, the transmission coefficients were slightly smaller for the Diels−Alder reaction: $\kappa = 0.95$ in the gas phase and $\kappa = 0.89$ in the presence of two water molecules. The smaller transmission coefficients for the Diels−Alder reactions are due mainly to the flatter potential energy along the reaction coordinate near the transition state and the closer proximity of the coupling peak to the transition state. These differences lead to lower momentum along the reaction coordinate in the strong coupling region and, thus, a higher probability of reflections. The decrease in the transmission coefficient for the Diels−Alder reaction in the presence of two water molecules is due to a combination of a flatter potential energy along the reaction coordinate near the transition state and a larger curvature peak on the product side.

In general, dynamical solvation effects decrease the transmission coefficient when the inclusion of water molecules leads to the following effects: (1) a potential energy that is flatter near the transition state, (2) curvature peaks that are located closer to the transition state, (3) curvature peaks that are larger in magnitude, and (4) frequencies of the relevant orthogonal vibrational modes that are lower near the transition state. For the two reactions studied in this paper, however, the transmission

coefficient does not deviate significantly from unity. Hence, the dominant effect of solvation is the lowering of the free energy barrier. For these cases, standard transition state theory provides a reasonable description of the rates. Nevertheless, analysis of the dynamical trajectories provides insight into possible reaction mechanisms.

This investigation of the solvent effects for these two fundamental organic reactions elucidates the electrostatic and structural roles of the water molecules, as well as the critical nature of the dynamical solvent effects. This approach is less computationally intensive than full-scale molecular dynamics simulations but still provides some useful qualitative information about dynamical solvent effects. This approach will be particularly useful for comparative studies (i.e., for investigating the effects of different substituents on the solute or of different solvents).

These studies lay the groundwork for a number of future directions. For example, the dynamical effects of including additional explicit water molecules will be investigated. Eventually the solute will be immersed in a periodic box containing hundreds of explicit solvent molecules. The reaction path Hamiltonian will be used in conjunction with standard molecular mechanical potentials to simulate the molecular dynamics of such a system. These simulations will provide insight into bulk solvent effects.

Acknowledgment. This work was supported by the AFOSR Grant F49620-98-1-0209. S.H.S. is the recipient of a Ralph E. Powe ORAU Junior Faculty Enhancement Award, an Alfred P. Sloan Foundation Research Fellowship, and a Camille Dreyfus Teacher−Scholar Award.

References and Notes

(1) Schuler, F. W.; Murphy, G. W. *J. Am. Chem. Soc.* **1950**, *72*, 3155.
(2) Burrows, C. J.; Carpenter, B. K. *J. Am. Chem. Soc.* **1981**, *103*, 6983.
(3) Gajewski, J. J.; Jurayj, J.; Gande, D. R.; Kimbrough, M. E.; Ganem, B.; Carpenter, B. K. *J. Am. Chem. Soc.* **1987**, *109*, 1170.
(4) Brandes, E. B.; Grieco, P. A.; Gajewski, J. J. *J. Org. Chem.* **1989**, *54*, 515.
(5) Severance, D. L.; Jorgensen, W. *J. Am. Chem. Soc.* **1992**, *114*, 10966.
(6) Rideout, D. C.; Breslow, R. *J. Am. Chem. Soc.* **1980**, *102*, 7816.
(7) Breslow, R. *Acc. Chem. Res.* **1991**, *24*, 159.
(8) Cramer, C. J.; Truhlar, D. G. *J. Am. Chem. Soc.* **1992**, *114*, 8794.
(9) Ruiz-Lopez, M. J.; Assfeld, X.; Garcia, J. I.; Mayoral, J. A.; Salvatella, L. *J. Am. Chem. Soc.* **1993**, *115*, 8780.
(10) Cativiela, C.; Dillet, V.; Garcia, J. I.; Mayoral, J. A.; Ruiz-Lopez, M. F.; Salvatella, L. *J. Mol. Struct. (THEOCHEM)* **1995**, *331*, 37.
(11) Storer, J. W.; Giesen, D. J.; Hawkins, G. D.; Lynch, G. C.; Cramer, C. J.; Truhlar, D. G.; Liotard, D. A. In Structure and Reactivity in Aqueous Solution: Characterization of Chemical and Biological Systems; Cramer, C. J., Truhlar, D. G., Eds.; American Chemical Society: Washington, D.C., 1994.
(12) Davidson, M. M.; Hillier, I. H.; Hall, R. J.; Burton, N. A. *J. Am. Chem. Soc.* **1994**, *116*, 9294.
(13) Hall, R. J.; Davidson, M. M.; Burton, N. A.; Hillier, I. H. *J. Phys. Chem.* **1995**, *99*, 921.
(14) Davidson, M. M.; Hillier, I. H. *J. Phys. Chem.* **1995**, *99*, 6748.
(15) Blake, J. F.; Jorgensen, W. L. *J. Am. Chem. Soc.* **1991**, *113*, 7430.
(16) Jorgensen, W. L.; Blake, J. F.; Lim, D.; Severance, D. L. *J. Chem. Soc., Faraday Trans.* **1994**, *90*, 1727.
(17) Severance, D. L.; Jorgensen, W. L. In Structure and Reactivity in Aqueous Solution: Characterization of Chemical and Biological Systems; Cramer, C. J., Truhlar, D. G., Eds.; American Chemical Society: Washington D.C., 1994.
(18) Gao, J. *J. Am. Chem. Soc.* **1994**, *116*, 1563.
(19) Gao, J.; Xia, X. In Structure and Reactivity in Aqueous Solution: Characterization of Chemical and Biological Systems; Cramer, C. J., Truhlar, D. G., Eds.; American Chemical Society: Washington D.C., 1994.
(20) Furlani, T. R.; Gao, J. *J. Org. Chem.* **1996**, *61*, 5492.
(21) Pak, Y.; Voth, G. A. *J. Phys. Chem. A* **1999**, *103*, 925.
(22) Chandler, D. *J. Chem. Phys.* **1978**, *68*, 2959.
(23) Miller, W. H.; Handy, N. C.; Adams, J. E. *J. Chem. Phys.* **1980**, *72*, 99.
(24) Dunning, T. H.; Kraka, E.; Eades, R. A. *Faraday Discuss.* **1987**, *84*, 427.
(25) Page, M.; McIver, J. W. *J. Chem. Phys.* **1988**, *88*, 922.
(26) Bell, R. L.; Taveras, D. L.; Truong, T. N.; Simons, J. *Int. J. Quantum Chem.* **1997**, *63*, 861.
(27) Keck, J. C. *J. Chem. Phys.* **1960**, *32*, 1035.
(28) Keck, J. C. *Discuss. Faraday Soc.* **1962**, *33*, 173.
(29) Anderson, J. B. *Advances in Chemical Physics*; Prigogine, I., Rice, S. A., Eds.; John Wiley & Sons: New York, 1995; Vol. XCI.
(30) Frisch, M. J.; Trucks, G. W.; Schlegel, H. B.; Scuseria, G. E.; Robb, M. A.; Cheeseman, J. R.; Zakrzewski, V. G.; Montgomery, J. A., Jr.; Stratmann, R. E.; Burant, J. C.; Dapprich, S.; Millam, J. M.; Daniels, A. D.; Kudin, K. N.; Strain, M. C.; Farkas, O.; Tomasi, J.; Barone, V.; Cossi, M.; Cammi, R.; Mennucci, B.; Pomelli, C.; Adamo, C.; Clifford, S.; Ochterski, J.; Petersson, G. A.; Ayala, P. Y.; Cui, Q.; Morokuma, K.; Malick, D. K.; Rabuck, A. D.; Raghavachari, K.; Foresman, J. B.; Cioslowski, J.; Ortiz, J. V.; Stefanov, B. B.; Liu, G.; Liashenko, A.; Piskorz, P.; Komaromi, I.; Gomperts, R.; Martin, R. L.; Fox, D. J.; Keith, T.; Al-Laham, M. A.; Peng, C. Y.; Nanayakkara, A.; Gonzalez, C.; Challacombe, M.; Gill, P. M. W.; Johnson, B. G.; Chen, W.; Wong, M. W.; Andres, J. L.; Head-Gordon, M.; Replogle, E. S.; Pople, J. A. *Gaussian 98*, revision A.6; Gaussian, Inc.: Pittsburgh, PA, 1998.
(31) Ditchfield, R.; Hehre, W. J.; Pople, J. A. *J. Chem. Phys.* **1971**, *54*, 724.
(32) Hehre, W. J.; Ditchfield, R.; Pople, J. A. *J. Chem. Phys.* **1972**, *56*, 2257.
(33) Francl, M. M.; Petro, W. J.; Hehre, W. J.; Binkley, J. S.; Gordon, M. S.; DeFrees, D. J.; Pople, J. *A. J. Chem. Phys.* **1982**, *77*, 3654.
(34) Becke, A. D. *J. Chem. Phys.* **1993**, *98*, 1372.
(35) Stephens, P. J.; Devlin, F. J.; Chabalowski, C. F.; Frisch, M. J. *J. Phys. Chem.* **1994**, *98*, 11623.
(36) Becke, A. D. *Phys. Rev. A* **1988**, *38*, 3098.
(37) Lee, C.; Yang, W.; Parr, R. G. *Phys. Rev. B* **1988**, *37*, 785.
(38) Gonzales, C.; Schlegel, H. B. *J. Chem. Phys.* **1989**, *90*, 2154.
(39) Baboul, A. G.; Schlegel, H. B. *J. Chem. Phys.* **1997**, *107*, 9413.
(40) Breneman, C. M.; Wiberg, K. B. *J. Comput. Chem.* **1990**, *11*, 361.
(41) Press, W. H.; Flannery, B. P.; Teukolsky, S. A.; Vetterling, W. T. *Numerical Recipes in C*; Cambridge University Press: New York, 1988.
(42) Goldstein, H. *Classical Mechanics*, 2nd ed.; Addison-Wesley: Reading, MA, 1980.
(43) Yamashita, K.; Miller, W. H. *J. Chem. Phys.* **1985**, *82*, 5475.
(44) Wang, H.; Hase, W. L. *Chem. Phys.* **1996**, *212*, 247.
(45) Vance, R. L.; Rondan, N. G. *J. Am. Chem. Soc.* **1988**, *110*, 2314.
(46) Loncharich, R. J.; Brown, R. J.; Houk, K. N. *J. Org. Chem.* **1989**, *54*, 1129.
(47) Jorgensen, W. L.; Lim, D.; Blake, J. F. *J. Am. Chem. Soc.* **1993**, *115*, 2936.
(48) Wiest, O.; Black, K.; Houk, K. N. *J. Am. Chem. Soc.* **1994**, *116*, 10336.